Electronic Supplementary Material (ESI) for Journal of Materials Chemistry A.

Tetrahexahedral PdRh nanocrystals with tunable composition as highly efficient electrocatalyst for ethylene glycol oxidation

Jing-Xiao Tang, Liang-Ping Xiao, Chi Xiao, Na Tian,* Zhi-You Zhou and Shi-Gang Sun*

State Key Laboratory of Physical Chemistry of Solid Surfaces, Collaborative Innovation Center of Chemistry for Energy Materials, College of Chemistry and Chemical Engineering, Xiamen University, Xiamen 361005, China.

Chemicals and materials

Glassy-carbon electrode (99.99%, Φ = 6 mm) was purchased from Takai Carbon Co., LTD. (Tokyo, Japan). Commercial Pd/C (20 wt.%) was purchased from Alfa Aesar (Tianjin, China). NaOH, ethylene glycol and $PdCl_2$ were purchased from Sinopharm Chemical Reagent Co., LTD. (Shanghai, China). $RhCl_3$ was purchased from Aladdin Biochemical Technology Co., LTD. (Shanghai, China). Perchloric acid (EMSURE® ACS) was purchased from Merck. Argon (99.99%) and CO (99.9%) were purchased from Linde gas Co., LTD (Xiamen). All the chemicals were used as received without further purification. The ultra-pure water (18 MΩ cm) for cleaning glassware and solution preparation was produced from the Millipore system.

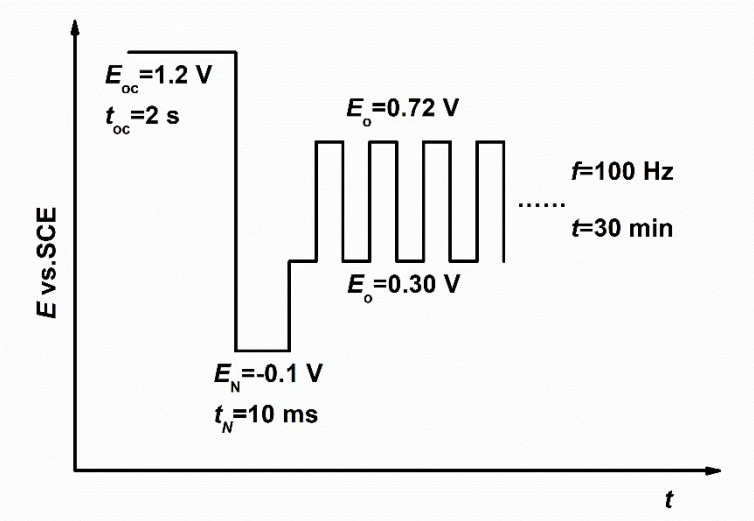

Fig. S1 Scheme of pulse waveform applied for preparation of THH PdRh NCs, THH Pd NCs, and Rh nanoparticles.

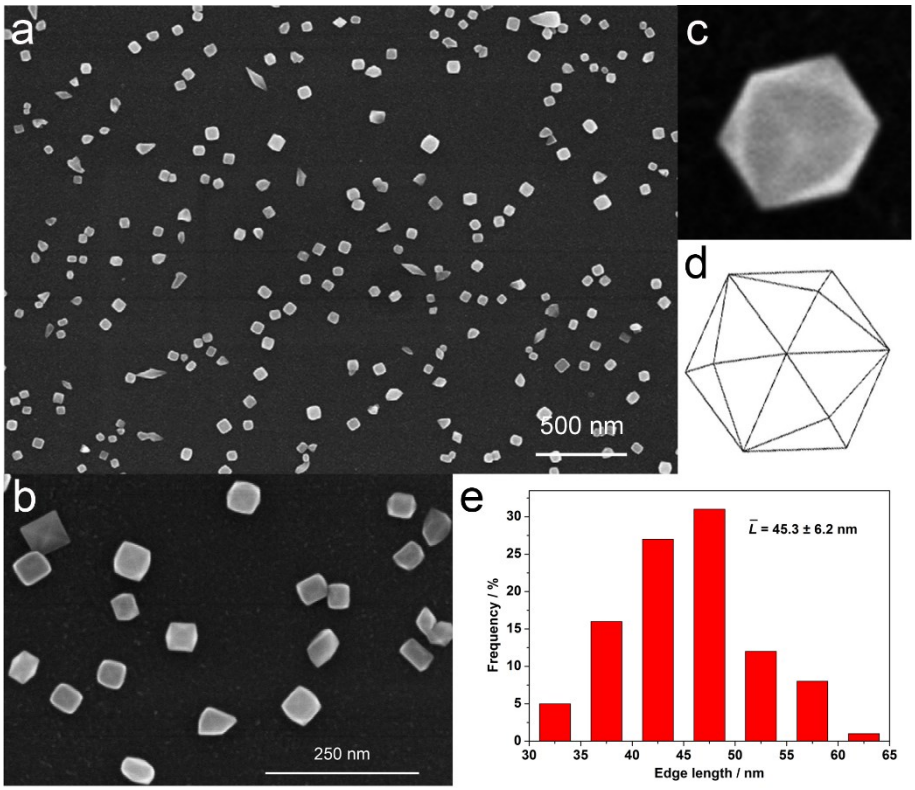

Fig. S2 (a, b) Low- and (c) high-magnification SEM images of THH $Pd_{86.9}Rh_{13.1}$ NCs. (d) Geometrical model of an ideal THH. (e) Histogram of edge length. The edge length distribution was determined by statistics of over 200 THH NCs.

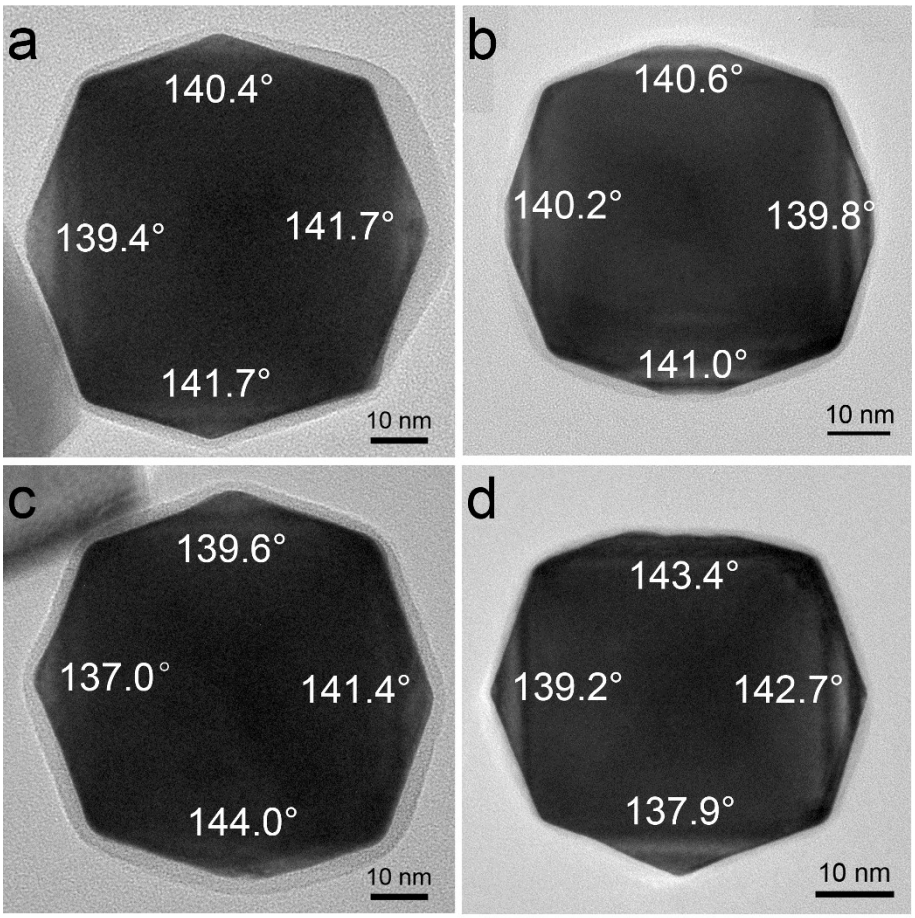

e

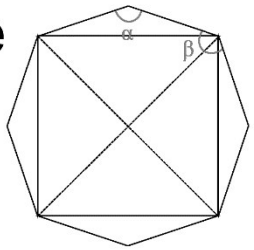

	α	β
{520}	136.4	133.6
{11 4 0}	140.0	130.0
{310}	143.1	126.9

Fig. S3 (a-d) TEM images of four individual THH $Pd_{86.9}Rh_{13.1}$ NCs captured along [001] crystal axis and their interfacial angles. (e) Theoretical interfacial angles of THH bounded by different {*hk*0} facets.

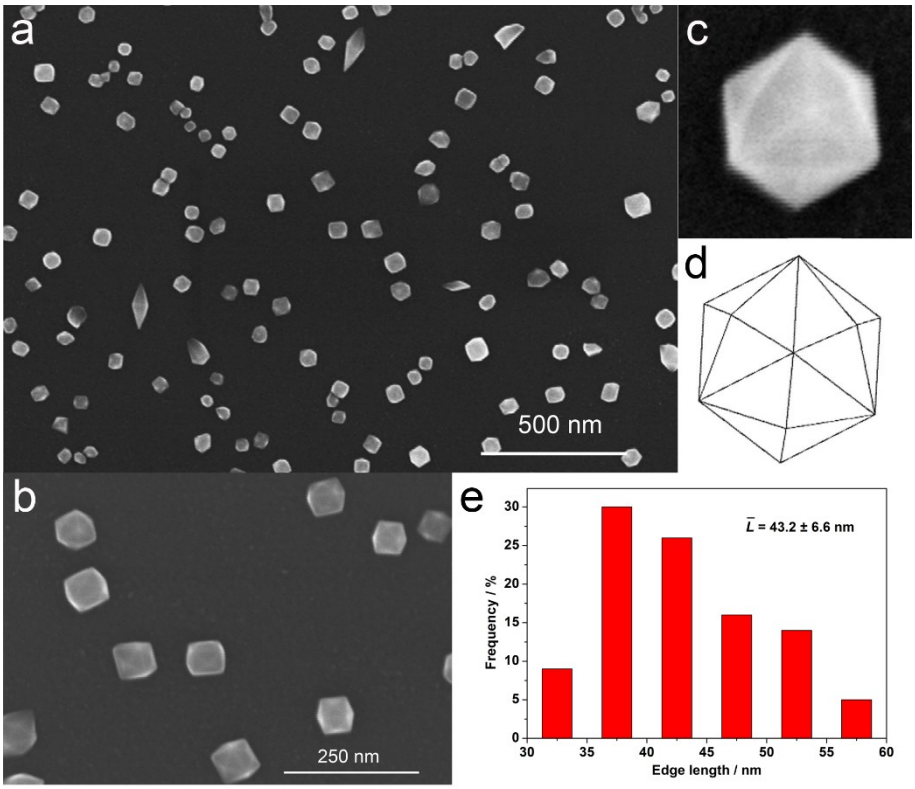

Fig. S4 (a, b) Low- and (c) high-magnification SEM images of THH $Pd_{90.1}Rh_{9.9}$ NCs. (d) Geometrical model of an ideal THH. (e) Histogram of edge length.

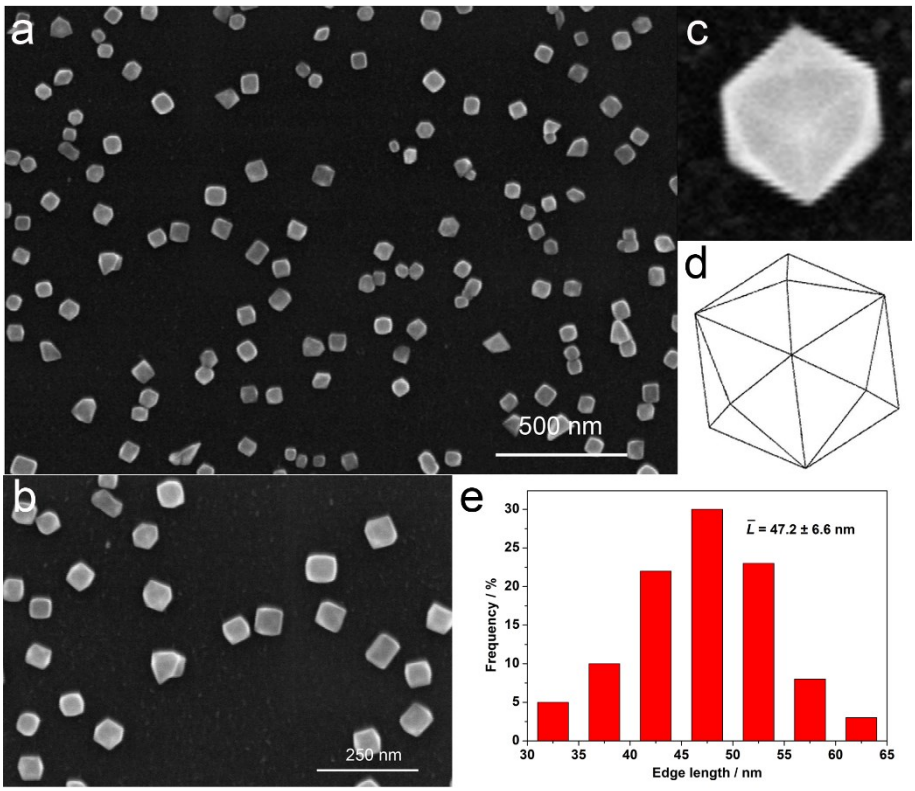

Fig. S5 (a, b) Low- and (c) high-magnification SEM images of THH $Pd_{92.8}Rh_{7.2}$ NCs. (d) Geometrical model of an ideal THH. (e) Histogram of edge length.

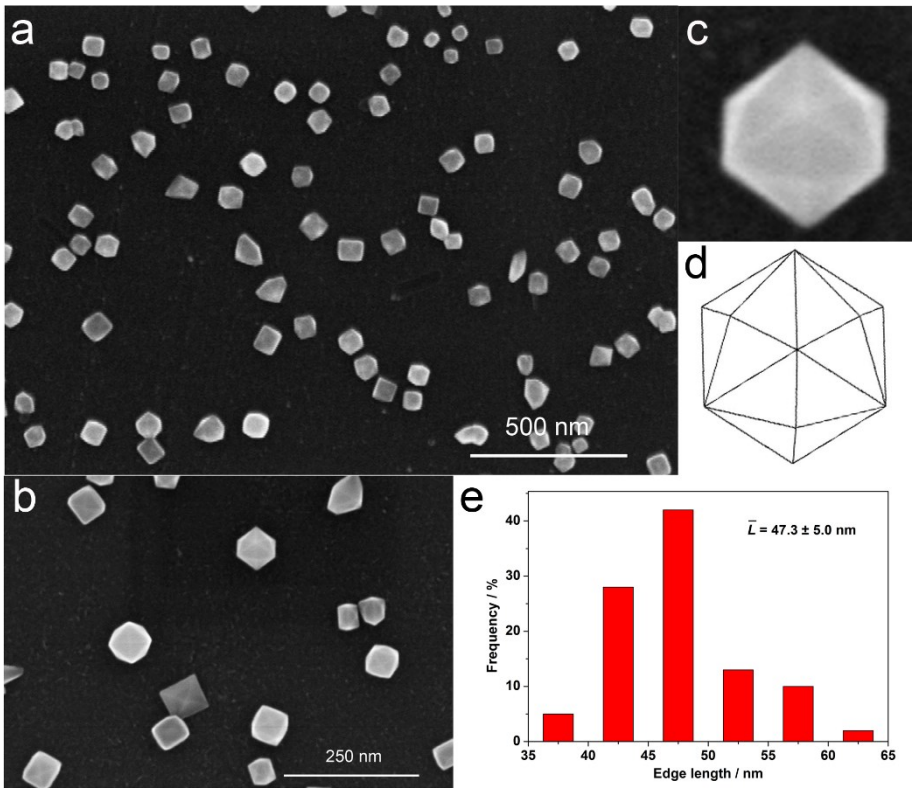

Fig. S6 (a, b) Low- and (c) high-magnification SEM images of THH $Pd_{94.6}Rh_{5.4}$ NCs. (d) Geometrical model of an ideal THH. (e) Histogram of edge length.

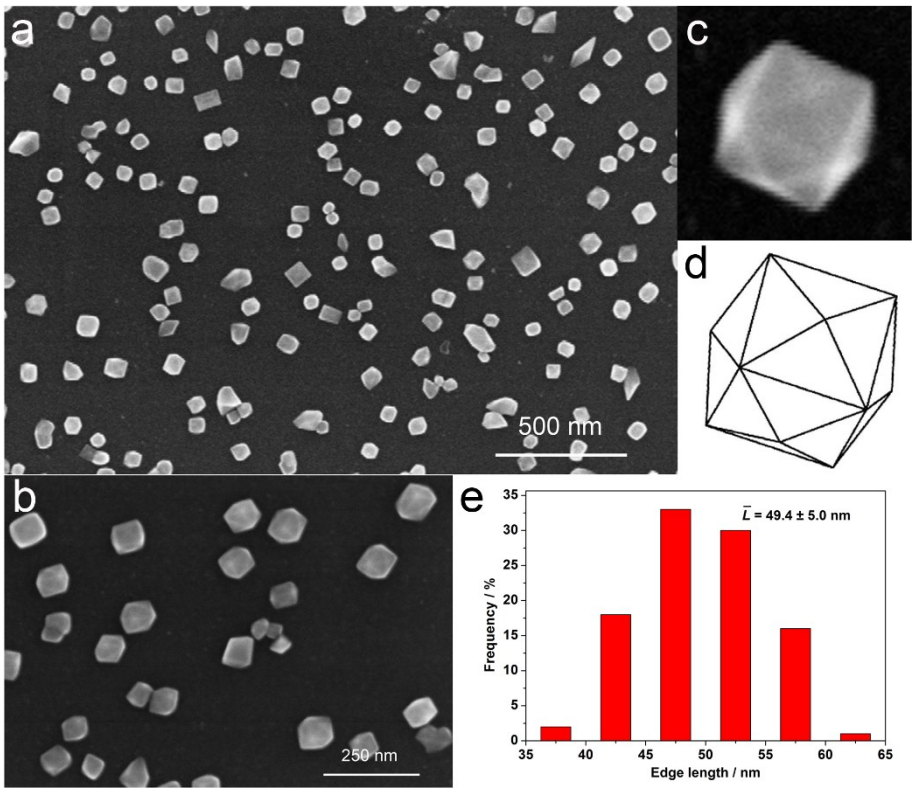

Fig. S7 (a, b) Low- and (c) high-magnification SEM images of THH Pd NCs. (d) Geometrical model of an ideal THH. (e) Histogram of edge length.

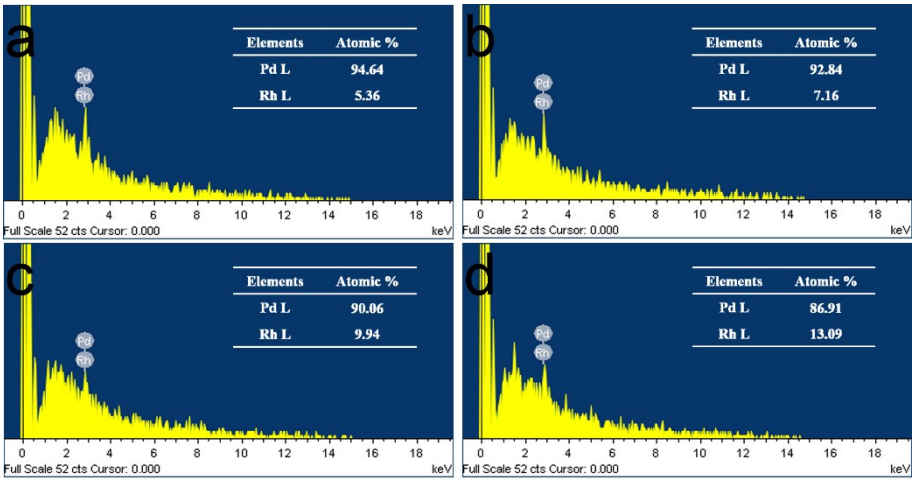

Fig. S8 EDS spectra of THH PdRh NCs. (a) THH $Pd_{94.6}Rh_{5.4}$NCs; (b) THH $Pd_{92.8}Rh_{7.2}$NCs; (c) THH $Pd_{90.1}Rh_{9.9}$ NCs; (d) THH $Pd_{86.9}Rh_{13.1}$ NCs.

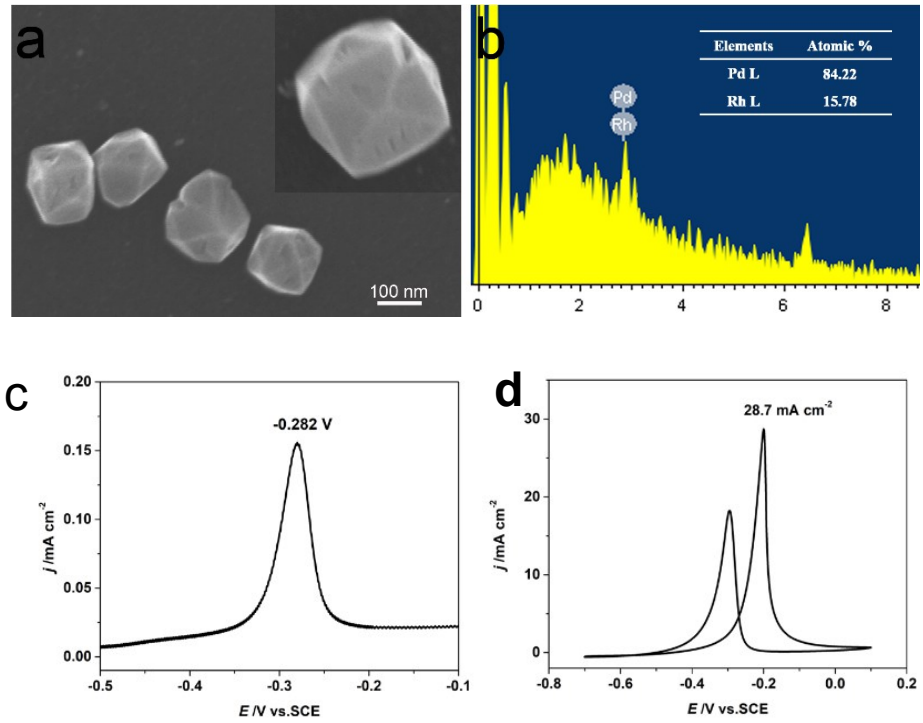

Fig. S9 (a) SEM image and (b) EDS of $Pd_{84.2}Rh_{15.8}$ NCs prepared in 0.2 mM $PdCl_2$ + 0.2 mM $RhCl_3$ solution. The THH shape is imperfect. (c) CO stripping on imperfect THH $Pd_{84.2}Rh_{15.8}$ NCs in 0.1 M NaOH. Scan rate: 20 mV s^{-1}. (d) Cyclic voltammogram of EG electrooxidation on imperfect THH $Pd_{84.2}Rh_{15.8}$ NCs in 1 M NaOH + 1 M EG solution at 50 mV s^{-1}.

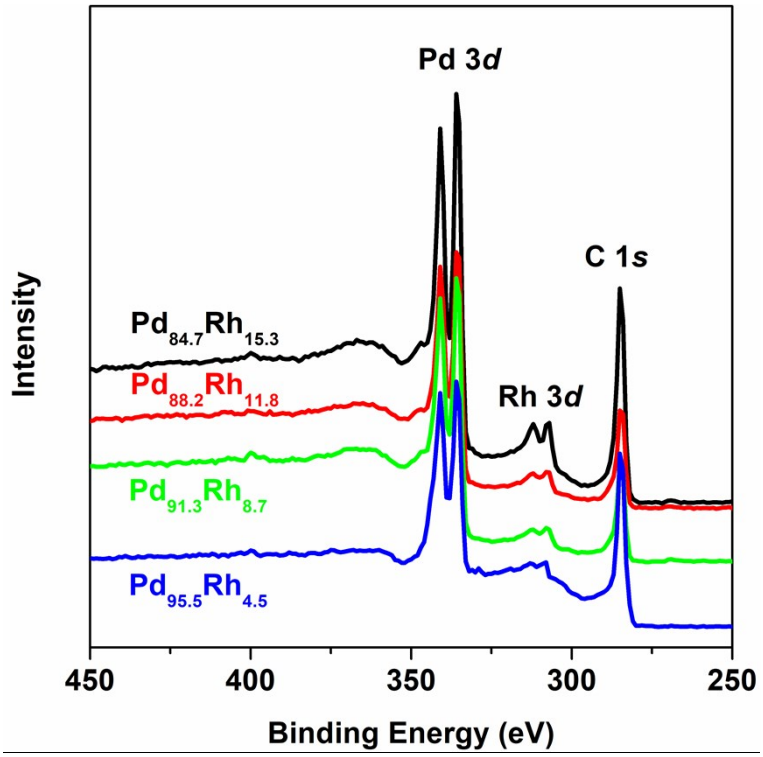

Fig. S10 XPS of THH PdRh NCs.

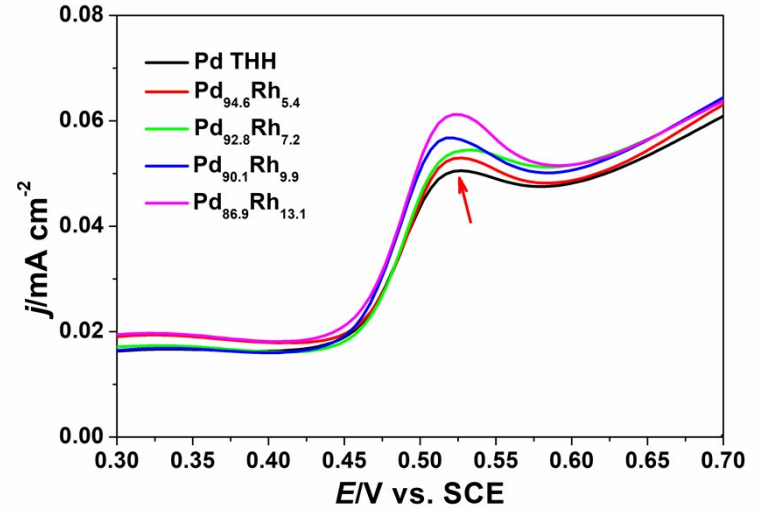

Fig. S11 Enlarged voltammograms of THH PdRh NCs and THH Pd NCs recorded in 0.1 M $HClO_4$. Scan rate: 50 mV s^{-1}.

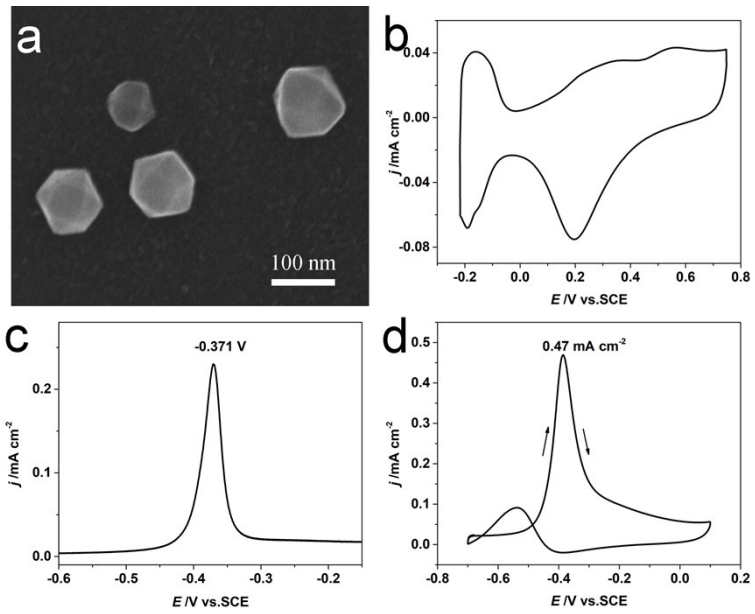

Fig. S12 (a) SEM image of THH Rh NCs. (b) Cyclic voltammogram of THH Rh NCs 0.1 M $HClO_4$. Scan rate: 50 mV s^{-1}. (c) CO stripping on THH Rh NCs. Scan rate: 20 mV s^{-1}. (d) Cyclic voltammogram of EG electrooxidation on THH Rh NCs in 1 M NaOH + 1 M EG solution at 50 mV s^{-1}.

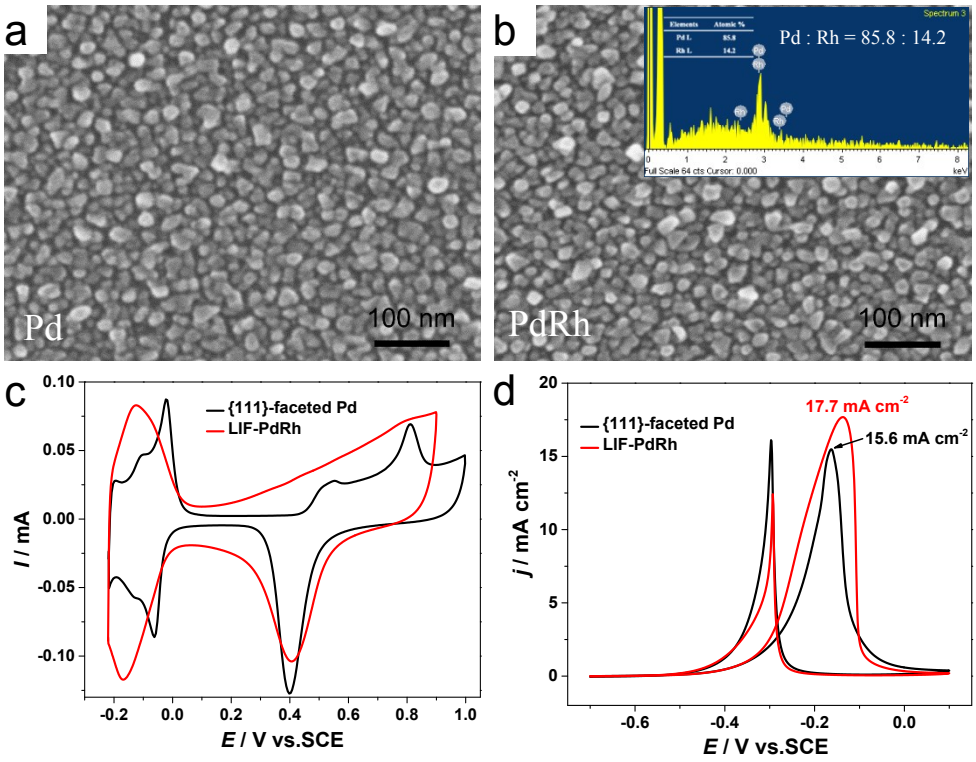

Fig. S13 (a, b) SEM images of {111}-faceted Pd NCs (a) and low-index faceted (LIF) PdRh NCs (b). inset is the EDS of LIF-PdRh NCs. (c) Cyclic voltammograms of {111}-faceted Pd and LIF-PdRh NCs recorded in 0.1 M $HClO_4$ at 50 mV s^{-1}. The Pd NCs show characteristic peak at about 0.80 V for oxygen species adsorption on Pd(111) [1]. (d) Cyclic voltammograms of EG electrooxidation on {111}-faceted Pd and LIF-PdRh NCs in 1 M NaOH + 1 M EG solution at 50 mV s^{-1}.

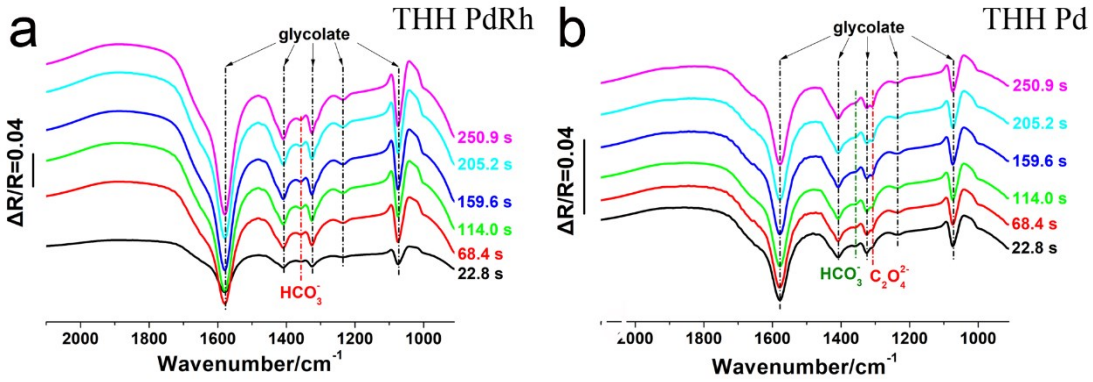

Fig. S14 TRFTIR spectra of THH $Pd_{86.9}Rh_{13.1}$ NCs (a) and THH Pd NCs (b) in 1 M EG + 1 M NaOH solution. E_S = −0.20 V, E_R = −0.70 V. Time interval: 45 s.

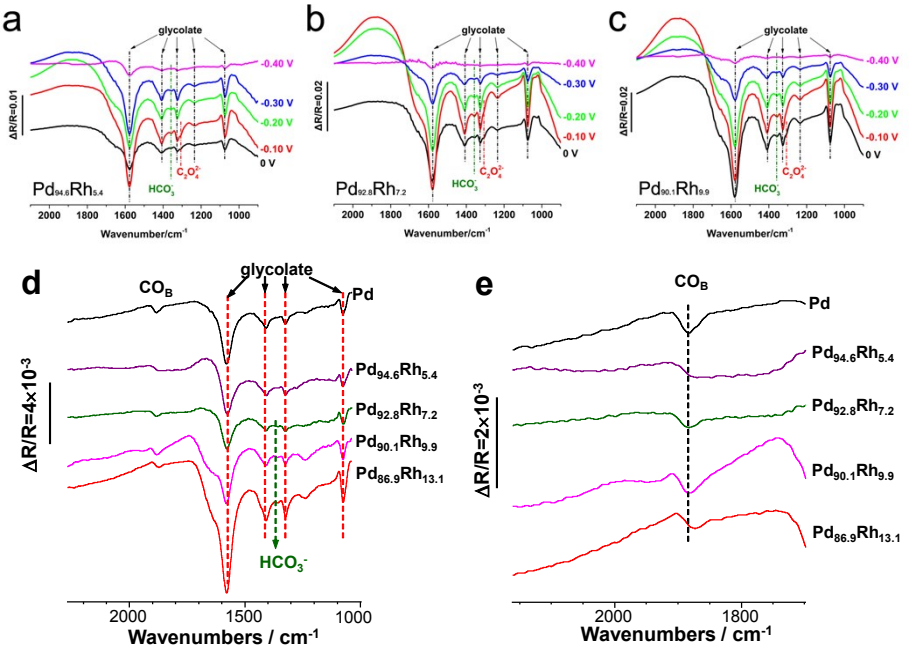

Fig. S15 In situ FTIR spectra of EG electrooxidation on (a) THH $Pd_{94.6}Rh_{5.4}$ NCs, (b) THH $Pd_{92.8}Rh_{7.2}$ NCs, and (c) THH $Pd_{90.1}Rh_{9.9}$ NCs at different potential. E_S = −0.40 ~ 0 V, E_R = −0.70 V, solution: 1 M EG + 1 M NaOH; Spectral resolution: 8 cm^{-1}. (d) Comparison of in situ FTIR spectra collected at −0.40 V for THH Pd NC and THH PdRh NCs. (b) Enlarged spectra of adsorbed CO. THH Pd NCs show more bridge-bonded CO (CO_B) than THH PdRh NCs.

Table S1 SEM-EDS and XPS results of THH PdRh NCs.

	Pd/Rh (EDS)	Pd/Rh (XPS)
$Pd_{94.6}Rh_{5.4}$	94.6:5.4	95.5:4.5
$Pd_{92.8}Rh_{7.2}$	92.8:7.2	91.3:8.7
$Pd_{90.1}Rh_{9.9}$	90.1:9.9	88.2:11.8
$Pd_{86.9}Rh_{13.1}$	86.9:13.1	84.7:15.3

Table S2 Binding energy (BE) and relative intensity obtained from Pd 3*d* and Rh 3*d* XPS spectra of THH $Pd_{86.9}Rh_{13.1}$ NCs.

Species	BE (eV)	Relative intensity (%)	Species	BE (eV)	Relative intensity (%)
Pd(0)	335.5	33.2	Rh(0)	307.4	51.9
$Pd(OH)_x$	335.9	34.2	Rh_2O_3	308.4	25.5
PdO	336.3	19.2	$RhCl_3$	310.2	22.6
PdO_2	338.0	13.4			

Table S3 Onset and peak potential of CO stripping and ECSA of different catalysts.

	E_{onset} / V	E_P / V	ECSA / cm^2
THH Pd NCs	−0.280	−0.191	0.135
$Pd_{94.6}Rh_{5.4}$	−0.314	−0.251	0.133
$Pd_{92.8}Rh_{7.2}$	−0.340	−0.263	0.124
$Pd_{90.1}Rh_{9.9}$	−0.350	−0.271	0.131
$Pd_{86.9}Rh_{13.1}$	−0.354	−0.278	0.123
Pd/C	−0.266	−0.151	0.823

Table S4 Comparison of catalytic performance for EG oxidation on different catalysts.

	$E_{P,f}$ / V	j_f / mA cm^{-2}	j_b / mA cm^{-2}
THH Pd NCs	−0.184	21.8	18.3
$Pd_{94.6}Rh_{5.4}$	−0.197	31.6	20.7
$Pd_{92.8}Rh_{7.2}$	−0.198	34.4	21.9
$Pd_{90.1}Rh_{9.9}$	−0.197	38.8	21.9
$Pd_{86.9}Rh_{13.1}$	−0.200	43.7	22.4
Pd/C	−0.149	3.93	3.21

$E_{p,f}$: Peak potential in the forward scan;

j_f: Peak current density in the forward scan;

j_b: Peak current density in the backward scan.

Table S5 Comparison of catalytic activities of various catalysts for EG electrooxidation.

Catalysts	Electrolyte	j_f / mA cm^{-2}	Refs
THH $Pd_{86.9}Rh_{13.1}$ NCs	1 M EG + 1 M NaOH	43.70	This work
Screw-like Pd_1Pt_1 nanowires	0.5 M EG + 0.5 M NaOH	16.93	2
$Pd_{55}Pt_{30}$ nanowires networks	0.5 M EG + 0.5 M KOH	15.19	3
$Pd_{62}Au_{21}Ni_{17}$ nanosponges	0.5 M EG + 0.5 M KOH	17	4
PtPdCo nanoflowers	0.5 M EG + 1 M KOH	7.22	5
PtPd@Pt NCs/rGO	0.5 M EG + 0.5 M KOH	1.88	6
PdPt nanodendrites	0.5 M EG + 1 M KOH	5.2	7
PdCo nanodendrites		3.33	
PdNi nanodendrites		1.83	
PdPt multipods	1 M EG + 1 M KOH	8.42	8
PtNi nanowires	0.5 M EG + 0.5 M KOH	9.6	9
PdPtNi nanowires		15.9	
PdNi nanowires		8.9	
Core-shell Pd_3Pb@Pd aerogels	0.5 M EG + 1 M KOH	15.31	10
Pt_4Rh nanocubes	1 M EG + 1 M KOH	11.6	11

All scan rates are 50 mV s^{-1}.

Table S6 IR bands and their assignment of EG electrooxidation on THH $Pd_{86.9}Rh_{13.1}$ NCs and THH Pd NCs.

Species	Band center / cm^{-1}
CO_B	1884
glycolate	1580, 1410, 1326, 1234, 1075
$C_2O_4^{2-}$	1308
HCO_3^-	1357

Supplementary References

[1] K. Sashikata, Y. Matsui, and K. Itaya, *J. Phys. Chem.*, 1996, **100**, 20027–20034.

[2] J. X. Tang, Q. S. Chen, L. X. You, H. G. Liao, S. G. Sun, S. G. Zhou, Z. N. Xu, Y. M. Chen and G. C. Guo, *J. Mater. Chem. A*, 2018, **6**, 2327–2336.

[3] W. Hong, C. S. Shang, J. Wang, E. K. Wang, *Energy & Environ. Sci.*, 2015, **8**, 2910–2915.

[4] S. P. Li, J. P. Lai, R. Luque, G. B. Xu, *Energy & Environ. Sci.*, 2016, **9**, 3097–3102.

[5] P. Song, L. Liu, A. J. Wang, X. Zhang, S. Y. Zhou, J. J. Feng, *Electrochim. Acta*, 2015, **164**, 323–329.

[6] L. Liu, X. X. Lin, S. Y. Zou, A. J. Wang, J. R. Chen, J. J. Feng, *Electrochim. Acta*, 2016, **187**, 576–583.

[7] J. N. Zheng, L. L. He, F. Y. Chen, A. J. Wang, M. W. Xue, J. J. Feng, *J. Mater. Chem. A*, 2014, **2**, 12899–12906.

[8] J. J. Lv, L. P. Mei, X. X Weng, A. J. Wang, L. L. Chen, X. F. Liu, J. J. Feng, *Nanoscale*, 2015, **7**, 5699–5705.

[9] Y. Wang, T. Y. Kou, H. Gao, J. Z. Niu, J. Zhang, L. F. Lv, Z. Q Peng, Z. H. Zhang, *J. Mater. Chem. A*, 2018, **6**, 10525–10534.

[10] C. Z. Zhu, Q. R. Shi, S. F. Fu, J. H. Song, D. Du, D. Su, M. H. Engelhard, Y. H. Lin, *J. Mater. Chem. A*, 2018, **6**, 7517–7521.

[11] F. Gao, Y. P. Zhang, P. P. Song, J. Wang, T. X Song, C. Wang, L. Song, Y. Shiraishi, Y. K. Du, *J. Mater. Chem. A*, 2019, **7**, 7891–7896.